Communications

Bilayer Interdiffused Heterojunction Organic Photodiodes Fabricated By Double Transfer Stamping

Hyunsoo Kim[a], Byeongseop Song[a], Kyusang Lee[c,d], Stephen Forrest[a,b] and Jerzy Kanicki[a,*]

[a]Department of Electrical Engineering and Computer Science, University of Michigan, Ann Arbor, MI

48109, USA

[b]Department of Physics, University of Michigan, Ann Arbor, MI 48109, USA

[c]Department of Electrical and Computer Engineering, University of Virginia, Charlottesville, VA

22904, USA

[d]Department of Material Science and Engineering, University of Virginia, Charlottesville, VA 22904,

USA

*email: kanicki@umich.edu

Abstract

We demonstrate a double transfer stamping method for the fabrication of a bilayer, interdiffused organic photodetector. The approach leads to a device having both a low dark current and high photoresponsivity through optimization of the metal-organic interfaces and segregation of electron donor and acceptor materials within the device active layer. Dark current densities as low as 7.7 ± 0.3 nA/cm^2 and external quantum efficiencies of 60 ± 1 % are achieved with a calculated specific detectivity of $(4.8 \pm 0.2) \times 10^{12}$ cm·Hz$^{1/2}$W^{-1} at a reverse bias of 1.5 V and wavelength of 546 nm. The organic photodiodes also show a linear dynamic range of > 120 dB.

1. Introduction

Photodetctors based on organic materials have attracted attention due to their wide spectral response,[1–3] low dark current density,[4,5] high photoresponse[6,7] and fast response time.[8] In particular, bulk heterojunctions (BHJs) have been exploited in organic photodetectors (OPD) due to their high photocarrier generation efficiency and simplified solution-based fabrication.[9,10] However, the co-existence of the donor and acceptor materials at the cathode and anode interfaces can lead to high dark currents due to formation of low barrier heights for carrier injection, leading to shunt currents.[10] Dark current suppression can be achieved, in principle, by controlling donor/acceptor (D/A) segregation using a double active layer structure.[4,11] To fabricate the bilayer using a solution process, "orthogonal" solvents are required for each material to avoid resolution of an already-deposited layer.[12] Ayzner et al. reported that o-dichlorobenzene (DCB) and dichloromethane (DCM) are orthogonal solvents useful in the sequential deposition of poly(3-

hexylthiophene) (P3HT) and [6,6]-phenyl C61-butyric acid methyl ester (PCBM) layer.[13] This approach nevertheless allows partial mixing of the materials due to swelling of the P3HT by DCM used in depositing the PCBM.[14–17] This induces micro-penetration of each material to the counter-electrodes, forming current pathways resulting in shunt currents. An alternative is to use a silicon wafer treated with a releasing agent as a stamp to transfer one layer from the silicon wafer on top of another layer located on the target substrate, but this can result in surface contamination.[18,19] To minimize these adverse effects, the lamination process to the target substrate using a polydimethylsiloxane (PDMS) stamp treated in an O_2 plasma enables the spin-casting of a polymer film directly onto the PDMS stamp.[20] However, O_2 plasma treatment results in an increase of stamp surface adhesive energy, preventing efficient layer transfer from the PDMS to the substrate.

To address these problems, we introduce double transfer stamping (DTS) to promote interdiffusion between donor and acceptor layers to form well-defined interdiffused bilayer heterojunction (BiHJ) OPDs sandwiched between doner and acceptor layers that are in direct contact with their respective metal electrodes. The thermal annealing step is used to enable interdiffusion between the donor and acceptor layers, forming the active layer. Using this approach, we demonstrate an inverted interdiffused P3HT/PCBM bilayer photodiode whose dark current density is 7.7 ± 0.3 nA/cm^2 with an external quantum efficiency of 60 ± 1 % and a peak specific detectivity of (4.8 ± 0.2) x 10^{12} $cm \cdot Hz^{1/2}W^{-1}$.

2. Results and Discussion

In **Figure 1**, we show the energy level diagram for the OPD to illustrate how donor and acceptor bilayer interdiffusion can effectively suppress the dark current under reverse bias while maintaining a high quantum efficiency; the energy values shown are found elsewhere.[21] Although other approaches have been demonstrated to suppress dark current injection such as addition of a hole blocking layer (HBL) (e.g. ZnO)[21,22] at the anode, or an electron blocking layer (EBL) (e.g. Poly[N , N ′ -bis(4-butylphenyl)- N , N ′ -bis(phenyl)-benzidine] (poly-TPD)) at the cathode[2], the success of these methods are fabrication process dependent since the additional layers can introduce interface states that adversely affect device performance.[23–25] A simple and reliable means to suppress the reverse-biased dark current, therefore, is to have only the acceptor material in contact with the cathode while only donor material contacts the anode.[4,10] In the inverted BHJ in Figure 1(a), the hole injection barrier at the cathode is ΔE_{hole} = 1.4 eV (equal to the difference between the highest occupied molecular orbital, HOMO, energy of P3HT at 5.0 eV[26] and $\Phi_{ITO/PEIE}$ = 3.6 eV[27]), and the electron injection barrier at the anode is $\Delta E_{electron}$ = 2.6 eV (equal to the difference between Φ_{MoO3} 6.9 eV[28] and the lowest unoccupied MO, LUMO, energy of PCBM of 4.3 eV[26]). A significant increase of the barrier height is obtained by the formation of the bilayer HJ in Figure 1(b). Then the hole injection barrier at the cathode/PCBM interface is ΔE_{hole} = 2.5 eV (equal to the difference between the HOMO energy of PCBM of 6.1 eV[26] and $\Phi_{ITO/PEIE}$) and the electron injection barrier at the anode/P3HT layer is $\Delta E_{electron}$ = 3.9 eV (equal to the difference between Φ_{MoO3}[28] and the LUMO energy of P3HT of 3.0 eV[26]). We expect that the increased ΔE_{hole} and $\Delta E_{electron}$ at cathode/anode interfaces reduces the dark leakage current while the lower energetic barrier (e.g. ΔE_{hole}) encourages current injection. The device structure is shown in Figure 1(c). The structure maximizes

the area of the D/A interfaces within a given volume via thermal interdiffusion, while maintaining undiluted electron donor and acceptor layer at the anode and cathode electrode, respectively.

Figure 2 illustrates the DTS fabrication process. Indium tin oxide (ITO) coated glass substrates were sequentially pre-cleaned by rinsing in acetone, isopropyl alcohol, and deionized water by sonication for 5 min, and then exposed to an oxygen plasma for 5 min. The low work function cathode was prepared by spin-coating polyethylenimine ethoxylated (PEIE) solution on the ITO coated glass[27] at 2000 rpm for 60 s, followed by thermal annealing at 100 ^{o}C for 10 min in air. This resulted in a <10 nm thick PEIE layer. The substrates were transferred into a glove box filled with N_2 gas (O_2, H_2O level < 0.5 ppm) for deposition of the photoactive layers. The PCBM in chlorobenzene (CB) solution was spin-coated for 60 s to form 90 ± 5 nm thick electron acceptor layer on the PEIE/ ITO substrate. To fabricate the PDMS stamp having suitable surface energy for the DTS process, contact angles were measured by dropping P3HT in CB solution on PDMS surfaces with varying elastomer-to-curing agent (E/C) ratios. The surface contact angles measured using a goniometer in air shown in Figure S1 decrease from 33 ± 3° to 18 ± 1° when the elastomer in PDMS ratio increases from 5:1 to 20:1, suggesting a decrease in PDMS surface hydrophobicity for increased E/C ratios. As the content of the cross-linker is reduced, the PDMS modulus of elasticity becomes too small to achieve the desired stiffness. We therefore employed PDMS stamps with 15:1 and 5:1 ratios of Sylgard elastomer and curing agent to achieve the optimal surface energy.

The P3HT solution was drop-cast in the glove box on a 5:1 PDMS stamp followed by combining with a 15:1 PDMS stamp to form a uniform polymer film between the two stamps by applying pressure. After room temperature solvent evaporation for about 10 s into the permeable stamp, the 15:1 PDMS stamp was detached. During this step, the P3HT polymer film is transferred

from 5:1 to 15:1 stamp having a higher adhesion. The thickness of the printed polymer film measured by surface profilometry is 90 ± 5 nm. Next, the polymer film formed on the 15:1 PDMS stamp was pressed onto the PCBM/PEIE/ITO to form a 190 ± 10 nm thick P3HT / PCBM bilayer. Following transfer, the bilayer is thermally annealed for 5 min at 70 ^{o}C to 150 ^{o}C, allowing the PCBM to diffuse into the P3HT film.[29] Finally, the devices were transferred into a thermal evaporator for deposition of a 15 nm MoO$_3$ / 100 nm Ag anode on the top of P3HT through an array of 1 mm diameter circular holes in shadow mask.

The ultraviolet-visible (UV-Vis) absorption spectra were measured for 200 nm thick as-cast and 110 ^{o}C BiHJ films, as shown **Figure 3(a)**. The absorption coefficients (α) of the as-cast, 110 ^{o}C BiHJ along with neat P3HT and PCBM films are plotted in **Figure 3(b)** versus photon energy. The broad absorption spectra of the as-cast and 110 ^{o}C BiHJ film are simply the superposition of the absorption of the P3HT and PCBM films. The 110 ^{o}C annealed BiHJ film showed a slight decrease of the P3HT absorption peak while PCBM absorption peak increased by 10 % compared to the as-cast BiHJ film. Overall, the spectra were similar over the entire wavelength region, with slight blue-shift of as-cast film relative to 110 ^{o}C film around 550 nm to 650 nm. The π-π* transition absorption peak for P3HT is observed from 450 nm to 550 nm[30] and the peak for PCBM at 345 nm.[31] The optical energy gaps (E_G) of as-cast and 110 ^{o}C annealed BiHJ film, estimated from the long wavelength absorption edges were about 1.90 ± 0.01 eV.[32]

The dark current density (J_d) versus applied voltage (V) characteristics changes with the thermal annealing conditions for the fabricated BiHJ OPDs is shown in **Figure 4**. The characteristics are fit (solid lines) with the modified diode equation for organic heterojunctions: [33]

6

$$J_d(V) = J_O \left[\exp\left(\frac{q(V - J_d(V)R_S A)}{nkT} \right) - 1 \right] + \frac{V - J_d(V)R_S A}{R_{sh}} \qquad (1)$$

Here , J_o is the dark saturation current density, A is the device area, n is the ideality factor, k is Boltzmann's constant, T is the temperature, R_S is the series resistance, and R_{sh} is the shunt resistance.

Higher dark currents observed for the as-cast device are due to residual solvent that can potentially introduce doping or traps, resulting in increased polaron pair recombination under reverse bias.[34,35] We observe that J_d at - 1.5 V decreases by more than one order of magnitude when the annealing temperature is increased to 110 °C. Annealing therefore leads to solvent evaporation from the film and interduffused layer formation. When the annealing temperature is 150 °C, we observe a sharp increase in J_d due to enhanced PCBM interdiffusion into P3HT, eventually penetrating to the counter-electrode (anode) and forming shunt current pathways.[29] This siginificantly reduces the carrier injection barrier (e.g. $\Delta E_{electron}$) at the cathode, leading to the observed increase in dark current at high reverse bias.

The capacitance-voltage (*C-V*) characteristics of the as-cast and 110 °C annealed BiHJ OPDs are shown in **Figure 5**. At high reverse bias, the capacitance for both devices saturates due to complete depletion of the organic layers,[36] leading to a geometric capacitance, $C_A = \varepsilon\varepsilon_0 A/t$, where the ε is the dielectric constant of active layer, ε_o is the vacuum permittivity, and t is layer thickness. The capacitances for the as-cast and 110 °C devices at -2 V bias are $C_{as\text{-}cast}$ = 153 pF and $C_{110^o C}$ = 123 pF, respectively (Fig. 5, inset). When the solvent is removed, the active layer thickness decreases by ~ 5 % (e.g. 190 ± 5 nm to 180 ± 5 nm). This should lead to $C_{110^o C} > C_{as\text{-}cast}$, which is opposite to observation. We attribute this to the change of layer morphology leading to a concomitant change in

the dielectric constant. Assuming that $C_{as\text{-}cast}$ is composed of two series-connected capacitors of P3HT and PCBM films of the same thickness, we can obtain:

$$C_{as-cast} = \frac{C_{P3HT}C_{PCBM}}{C_{P3HT}+C_{PCBM}} = \varepsilon_0 \frac{A}{t/2}\frac{\varepsilon_{P3HT}\varepsilon_{PCBM}}{\varepsilon_{P3HT}+\varepsilon_{PCBM}} \qquad (2)$$

where ε_{P3HT} = 4.4[37] and ε_{PCBM} = 3.9[38] are the dielectric constants of P3HT and PCBM films, respectively. The calculated $C_{as\text{-}cast}$ = 151 pF matches the experimental value, while the capacitance of the 110 °C annealed device can be approximated to $C_{110}{}^o{}_C = C_{BiHJ}$ due to the intermixed layer formed by annealing. Thus, the capacitance can be simplified as,

$$C_{110^oC} \approx C_{BiHJ} = \varepsilon_{BiHJ}\varepsilon_0 \frac{A}{t} \qquad (3)$$

where ε_{BiHJ} is the dielectric constant of the mixed P3HT:PCBM BiHJ film. The calculated ε_{BiHJ} based on the measured $C_{110}{}^o{}_C$ and thickness is 3.2, which is comparable to ε_{BiHJ} = 3.3 reported previously.[36] The smaller ε_{BiHJ} of the mixed layer compared to ε_{P3HT} and ε_{PCBM} is possibly due to the solvent removal (the dielectric constant of CB is 5.62[39]) by thermal annealing.

We evaluated the OPD performance under various intensities at λ = 546 nm wavelength which lies at the P3HT:PCBM BiHJ absorption peak. The semi-log *J-V* characteristic at 50 µW/cm² light intensity for devices prepared with different annealing conditions is shown in Figure 4. Photocurrents as a function of intensity at -1.5 V bias for 110 °C BiHJ OPD are shown in **Figure 6**(a). The figure indicates that the optimized BiHJ OPD can respond to irradiance levels as low as ~10 nW/cm² at which point the photoresponse is limited by the dark current.

The linear dynamic range (*LDR*) is defined as, *LDR* = 20log(J^*_{ph}/J_d) [dB] where J^*_{ph} is the photocurrent density of the OPD, deviating from linearity by 10 %.[40] **Figure 6**(b) shows the *LDR* of

the 110 $^{\circ}$C annealed OPD at -1.5 V and λ = 546 nm is > 120 dB; the OPD exhibits no apparent photocurrent saturation up to 0.1 W/cm^2 . [1]

Figure 7(a) compares the measured *EQE* of the as-cast and 110 $^{\circ}$C annealed OPDs for biases of 0 V, -1.5 V, -3 V and -4.5 V. The *EQE* of the as-cast device is considerably lower than the 110 $^{\circ}$C annealed device across the entire spectral range measured. The unannealed device shows a peak *EQE* = 12 ± 2 % at λ = 435 nm, while the 110 $^{\circ}$C BiHJ OPD showed the highest *EQE* = 62 ± 2 % at -4.5 V at λ = 555 nm.

To clarify the difference in peak wavelength locations, the optical field distribution in the device was calculated using the transfer matrix method[41], with results in **Figure 7**(b). For the as-cast device, we assumed partially interdiffused BiHJ network having a BiHJ layer thickness of 10 nm sandwiched between 90 nm thick P3HT and PCBM layers. The BiHJ 110 $^{\circ}$C device is assumed to have a 160 nm thick interdiffused BiHJ layer sandwiched between 10 nm thick P3HT and PCBM layers. For the as-cast device, we calculate a peak photon absorption from 400 nm to 450 nm at the interface of the D/A layers, gradually decreasing with increasing wavelength. This is consistent with the experimental *EQE* obtained for the as-cast device, which implies that absorption within the BHJ is the primary site for photogeneration. The absorption at λ = 400 nm within the PCBM layer and at λ = 600 nm in the P3HT layer generates excitons that rapidly recombine due to the absence of a D/A junction within a diffusion length of approximately 5 nm to 20 nm.[42,43] In contrast, 110 $^{\circ}$C annealed device showed broad overlapping regions of photon absorption from λ = 500 nm to 600 nm, contributing directly to photogeneration of carriers in the extended interdiffused D/A junction.

Finally, to characterize the performance of OPD, we evaluated the OPD figure of merit measured at λ = 546 nm and at an intensity of 50 µW/cm^2. The calculated FOMs of the OPDs (J_d, *EQE*, Responsivity ($\mathcal{R}$), Noise Equivalent Power (*NEP*) and Specific Detectivity (*D**)) are summarized in **Table 2**. The definition of each FOMs can be found in Supporting Information.[40] While the lowest J_d was achieved by annealing at 110 ^{o}C, and the highest observed for the 150 ^{o}C device, both devices have $\mathcal{R}$ = 240 ± 10 mA/W. The comparable $\mathcal{R}$ values confirms that annealing at 110 ^{o}C is sufficient to induce interdiffusion layer leading to the maximum photoresponse. The 110 ^{o}C device showed *D** = (4.82 ± 0.2) x 10^{12} cm·Hz$^{1/2}$W^{-1} due to the lowest dark current of J_d = (7.72 ± 0.3) x 10^{-9} A/cm^2 at -1.5 V., which is among the best reported values for P3HT:PCBM based heterojunction OPDs.[44–46]

3. Conclusion

We demonstrated the DTS transfer printing of organic photodiodes with controlled donor/acceptor interdiffused heterojunctions sandwiched between donor and acceptor layers. Thermal annealing maximized the D/A interface within a well-defined volume. We demonstrated an OPD with a specific detectivity of (4.82 ± 0.2) x 10^{12} cm·Hz$^{1/2}$W^{-1} at 1.5 V reverse bias with J_{dark} = (7.7 ± 0.3) x 10^{-9} A/cm^2 and EQE = 60 ± 1 %. The DTS method can be applied to a variety of fullerene / polymer heterojunction system. The processing method is expected to allow freedom in selecting solvent systems for numerous materials to achieve a desired active layer morphology within the bulk heterojunction.

Experimental

PDMS Stamp and Solution Preparation : PDMS stamps were prepared by mixing Sylgard 184 silicone elastomer (Dow Corning) and a curing agent in a clean roon (43 % relative humidity, 20 $^{\circ}$C temperature) environment.[47] Various ratios of Sylgard:curing agent by mass were prepared to yield a different surface energies. The two components were mixed for 10 min and degassed at ~ 0.4 psi for six hours before being poured onto plastic weighing boats and cured at room temperature for three days. The PDMS stamps were peeled off from the boats and then cut into 1.5 x 1.5 cm^2 pieces. The PDMS stamps thicknesses were ~5 mm. The PDMS stamps were attached to glass wafers for transfer. The PEIE solution was prepared by dissolving 5 wt% of PEIE (Sigma Aldrich) in 2-methoxyethanol (2ME, Sigma Aldrich) solvent in atmosphere. Two active layer solutions were prepared in a N$_2$-filled glove box: (1) P3HT solution : 14 mg of P3HT (Rieke Metals, ~91 % regioregularity) was dissolved in 1.5 mL of CB (Sigma Aldrich) solvent; and (2) PCBM solution : 25 mg of PCBM (American Dye Source, Purity: > 99.5%) was dissolved in 1 mL of CB. All solution were filtered by 0.45 μm syringe filter and then stirred by magnetic bar overnight at 70 $^{\circ}$C.

Measurements : Contact angle measurements used a contact angle goniometer (Ramé-Hart) in a clean room (43 % relative humidity, 20 $^{\circ}$C temperature). The static sessile drop method was used to measure the advancing angle of the P3HT in CB solution droplet on the PDMS stamps. Optical absorbance spectra of the BiHJ films were measured using an Agilent CARY-5E UV-vis spectrometer. Dark current density – voltage (*J-V*) characteristics were measured by HP2416A semiconductor measurement system with a probe station at room temperature in air. For the *J-V* measurement of the OPDs under illumination, we used a solar simulator (Oriel) equipped with a Xe lamp, a band pass filter with peak wavelength at 546 nm (FWHM = 10 nm) and a 4156C semiconductor parameter analyzer. The devices were located inside the glove box and illumination was via the glass substrate.

A liquid light guide (Newport, 5mm diameter) and a broadband mirror were used for illumination. The intensity of the monochromatic light was measured by a radiant power meter (70260, Newport) using the same configuration. External quantum efficiency was measured from 0 V to -4.5 V. Incident light from a tungsten halogen lamp passing through a monochromator was chopped at 200 Hz to illuminate the the device. The generated AC photocurrent was amplified by a current amplifier (KEITHLEY 428) and then detected by a lock-in amplifier (SRS 830, Stanford Research that also provided reverse bias. A UV-enhanced silicon photodetector (UV808, Newport) was used for the light intensity calibration. Capacitance – voltage (C-V) measurements were performed in air using HP4284A LCR meter at room temperature in the dark. The amplitude of the small-signal voltage for the C-V measurement was 25 mV with frequency of 1 kHz.

Optical Modeling : Optical simulations used the transfer matrix method [41,48]. The complex refractive index (n = n + ik) of each material was acquired by a spectroscopic ellipsometer (M-2000, J. A. Woollam) with a B-spline fitting function (Figure S3). The electric field and absorbed optical power distributions were calculated as previously [41].

Supporting Information

Supporting Information is available from the Wiley Online Library or from the author.

WILEY-VCH

References

[1]   X. Gong, M. Tong, Y. Xia, W. Cai, J. S. Moon, Y. Cao, G. Yu, C.-L. Shieh, B. Nilsson, A. J. Heeger, *Science* **2009**, *325*, 1665.

[2]   X. Zhou, D. Yang, D. Ma, *Adv. Opt. Mater.* **2015**, *3*, 1570.

[3]   C. H. Cheung, D. Y. Kim, J. Subbiah, C. M. Amb, J. R. Reynolds, F. So, *IEEE Trans. Electron Devices* **2014**, *61*, 3852.

[4]   P. E. Keivanidis, S.-H. H. Khong, P. K. H. Ho, N. C. Greenham, R. H. Friend, *Appl. Phys. Lett.* **2009**, *94*, 173303.

[5]   A. Pierre, I. Deckman, P. B. Lechêne, A. C. Arias, *Adv. Mater.* **2015**, *27*, 6411.

[6]   F. Guo, B. Yang, Y. Yuan, Z. Xiao, Q. Dong, Y. Bi, J. Huang, *Nat. Nanotechnol.* **2012**, *7*, 798.

[7]   X. Hu, K. Wang, C. Liu, T. Meng, Y. Dong, S. Liu, F. Huang, X. Gong, Y. Cao, *J. Mater. Chem. C* **2014**, *2*, 9592.

[8]   P. Peumans, V. Bulovic, S. R. Forrest, *Appl. Phys. Lett.* **2000**, *76*, 3855.

[9]   G. Yu, J. Gao, J. C. J. Hummelen, F. Wudl, A. J. Heeger, *Science (80-.).* **1995**, *270*, 1789.

[10]   K.-J. Baeg, M. Binda, D. Natali, M. Caironi, Y.-Y. Noh, *Adv. Mater.* **2013**, *25*, 4267.

[11]   M. Binda, A. Iacchetti, D. Natali, L. Beverina, M. Sassi, M. Sampietro, *Appl. Phys. Lett.* **2011**, *98*, 073303.

[12]   V. S. Gevaerts, L. J. A. Koster, M. M. Wienk, R. a J. Janssen, *ACS Appl. Mater. Interfaces* **2011**, *3*, 3252.

[13]   A. L. Ayzner, C. J. Tassone, S. H. Tolbert, B. J. Schwartz, *J. Phys. Chem. C* **2009**, *113*, 20050.

[14]   B. A. Collins, E. Gann, L. Guignard, X. He, C. R. McNeill, H. Ade, *J. Phys. Chem. Lett.* **2010**, *1*, 3160.

[15]   K. H. Lee, P. E. Schwenn, A. R. G. Smith, H. Cavaye, P. E. Shaw, M. James, K. B. Krueger, I. R. Gentle, P. Meredith, P. L. Burn, *Adv. Mater.* **2011**, *23*, 766.

[16]   J. S. Moon, C. J. Takacs, Y. Sun, A. J. Heeger, *Nano Lett.* **2011**, *11*, 1036.

13

[17]   D. Chen, A. Nakahara, D. Wei, D. Nordlund, T. P. Russell, *Nano Lett.* **2011**, *11*, 561.

[18]   H. W. Ro, B. Akgun, B. T. O'Connor, M. Hammond, R. J. Kline, C. R. Snyder, S. K. Satija, A. L. Ayzner, M. F. Toney, C. L. Soles, D. M. DeLongchamp, *Macromolecules* **2012**, *45*, 6587.

[19]   D. Leman, M. A. Kelly, S. Ness, S. Engmann, A. Herzing, C. Snyder, H. W. Ro, R. J. Kline, D. M. DeLongchamp, L. J. Richter, *Macromolecules* **2015**, *48*, 383.

[20]   B. L. Chen, P. Degenaar, D. D. C. Bradley, *Adv. Mater.* **2008**, *20*, 1679.

[21]   H. Kim, K.-T. Lee, C. Zhao, L. J. Guo, J. Kanicki, *Org. Electron.* **2015**, *20*, 103.

[22]   H.-L. Yip, A. K.-Y. Jen, *Energy Environ. Sci.* **2012**, *5*, 5994.

[23]   F. Arca, S. F. Tedde, M. Sramek, J. Rauh, P. Lugli, O. Hayden, *Sci. Rep.* **2013**, *3*, 1324.

[24]   S. Dongaonkar, J. D. Servaites, G. M. Ford, S. Loser, J. Moore, R. M. Gelfand, H. Mohseni, H. W. Hillhouse, R. Agrawal, M. a. Ratner, T. J. Marks, M. S. Lundstrom, M. a. Alam, *J. Appl. Phys.* **2010**, *108*, 124509.

[25]   B. V. Popescu, D. H. Popescu, P. Lugli, S. Locci, F. Arca, S. F. Tedde, M. Sramek, O. Hayden, *IEEE Trans. Electron Devices* **2013**, *60*, 1975.

[26]   I. Hwang, D. Moses, A. J. Heeger, *J. Phys. Chem. C* **2008**, *112*, 4350.

[27]   Y. Zhou, C. Fuentes-Hernandez, J. Shim, J. Meyer, A. J. Giordano, H. Li, P. Winget, T. Papadopoulos, H. Cheun, J. Kim, M. Fenoll, A. Dindar, W. Haske, E. Najafabadi, T. M. Khan, H. Sojoudi, S. Barlow, S. Graham, J.-L. Brédas, S. R. Marder, A. Kahn, B. Kippelen, *Science* **2012**, *336*, 327.

[28]   J. Meyer, A. Kahn, *J. Photonics Energy* **2011**, *1*, 011109.

[29]   N. D. Treat, M. A. Brady, G. Smith, M. F. Toney, E. J. Kramer, C. J. Hawker, M. L. Chabinyc, *Adv. Energy Mater.* **2011**, *1*, 82.

[30]   H. Sirringhaus, P. J. Brown, R. H. Friend, M. M. Nielsen, *Nature* **1999**, 685.

[31]   V. Shrotriya, J. Ouyang, R. J. Tseng, G. Li, Y. Yang, *Chem. Phys. Lett.* **2005**, *411*, 138.

[32]   R. Kroon, M. Lenes, J. C. Hummelen, P. W. M. Blom, B. de Boer, *Polymer Reviews* **2008**, 48.3

[33]   N. C. Giebink, B. E. Lassiter, G. P. Wiederrecht, M. R. Wasielewski, S. R. Forrest, *Phys. Rev. B - Condens. Matter Mater. Phys.* **2010**, *82*, 1.

[34]   S. M. Sze, *Physics of semiconductor devices*; Wiley-Interscience, **2007**.

[35]   Robert F. Pierret, *Semiconductor Device Fundamentals*; Addison-Wesley, **1996**.

[36]   M. Mingebach, C. Deibel, V. Dyakonov, *Phys. Rev. B - Condens. Matter Mater. Phys.* **2011**, *84*, 1.

[37]   Y.-S. S. Cho, R. R. Franklin, *Trans. Electr. Electron. Mater.* **2012**, *13*, 237.

[38]   F. Jahani, S. Torabi, R. C. Chiechi, L. Jan, A. Koster, J. C. Hummelen, *Chem. Commun.* **2014**, *50*, 10645.

[39]   C. Wohlfarth, Springer Berlin Heidelberg, **2008**; pp. 323–325.

[40]   J.-M. Liu, *Photonic devices*; Cambridge University Press, **2005**.

[41]   L. A. A. Pettersson, L. S. Roman, O. Inganäs, *J. Appl. Phys.* **1999**, *86*, 487.

[42]   P. E. Shaw, A. Ruseckas, I. D. W. Samuel, *Adv. Mater.* **2008**, *20*, 3516.

[43]   G. F. Burkhard, E. T. Hoke, S. R. Scully, M. D. McGehee, *Nano Lett.* **2009**, *9*, 4037.

[44]   M. Ramuz, L. Bürgi, C. Winnewisser, P. Seitz, *Org. Electron.* **2008**, *9*, 369.

[45]   D. Baierl, B. Fabel, P. Gabos, L. Pancheri, P. Lugli, G. Scarpa, *Org. Electron.* **2010**, *11*, 1199.

[46]   S. F. Tedde, J. Kern, T. Sterzl, J. Fu, P. Lugli, O. Hayden, *Nano Lett.* **2009**, *9*, 980.

[47]   Y. Xia, G. M. Whitesides, *Annu. Rev. Mater. Sci.* **1998**, *28*, 153.

[48]   P. Peumans, A. Yakimov, S. R. Forrest, *J. Appl. Phys.* **2003**, *93*, 3693.

15

Table 1. The fit parameters for the BiHJ OPDs with different annealing conditions

Annealing conditions	J_d (A/cm^2) @ -1.5V	RshA (Ωcm^2)	RsA (Ωcm^2)	n	Jo (A/cm^2)
As-cast	9.38×10^{-8}	1.5×10^{7}	55	1.3	3.0×10^{-9}
70 °C	3.32×10^{-8}	4.0×10^{7}	50	1.45	1.5×10^{-9}
110 °C	7.72×10^{-9}	1.8×10^{8}	12	1.5	3.0×10^{-10}

Table 2. Performance of OPDs with different annealing conditions at irradiance of 50μW/cm^2 at 546 nm wavelength.

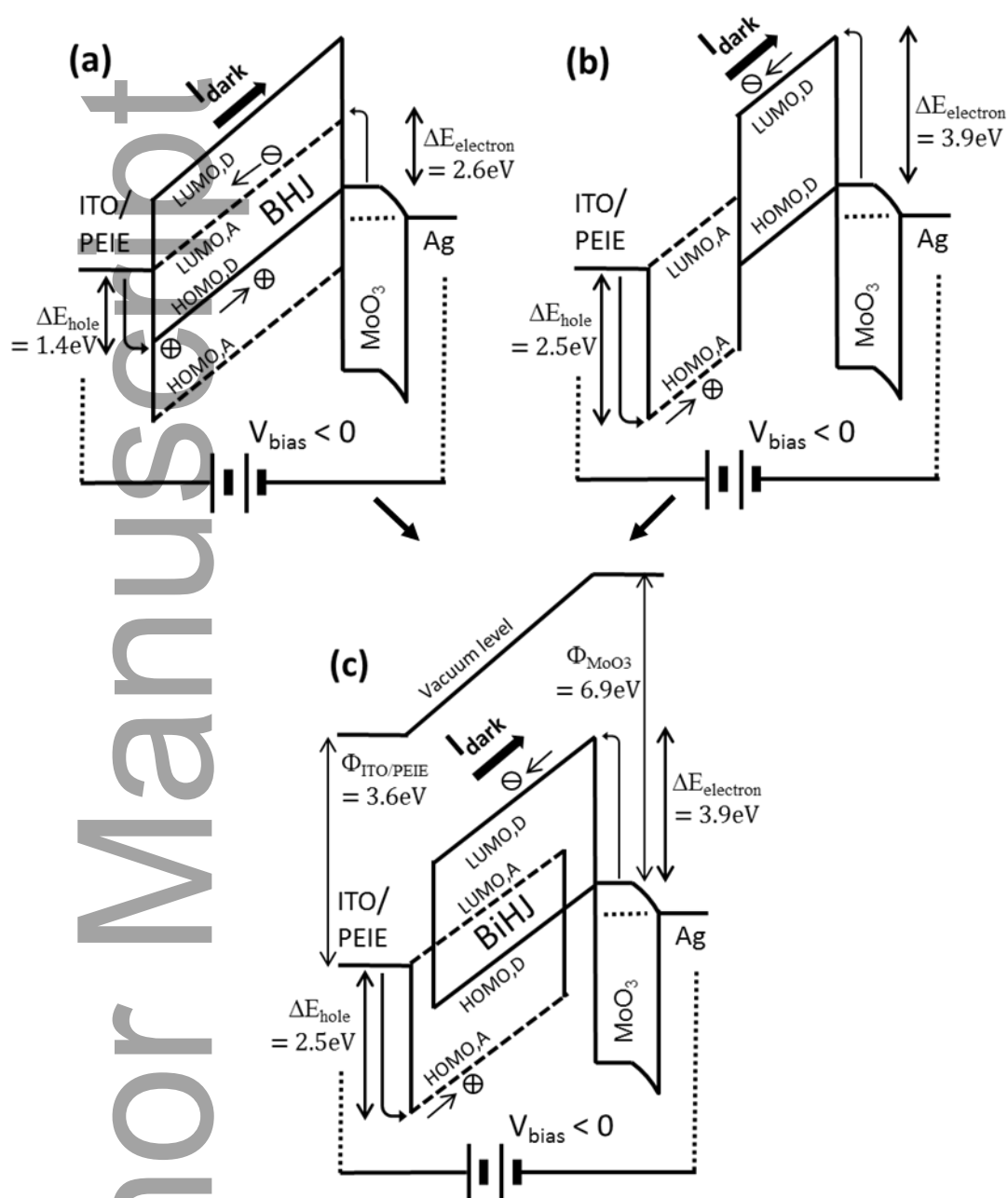| Annealing conditions	$\mathcal{R}$ (mA/W) @ -1.5V	EQE (%) @ -1.5V	NEP (W/Hz$^{1/2}$) @ -1.5V	D* (cm·Hz$^{1/2}$W^{-1}) @ -1.5V
As-cast	28	8	5.51×10^{-13}	1.61×10^{11}
70 °C	75	14	1.38×10^{-13}	6.44×10^{11}
110 °C	240	60	1.84×10^{-14}	4.82×10^{12}
150 °C	243	61	2.59×10^{-13}	3.42×10^{11}

Figure 1. Schematic energy diagrams of the (a) conventional bulkheterojunction (BHJ) OPD (b) bilayer OPD and (c) bilayer interdiffused heterojunction (BiHJ) OPD under reverse bias. The arrows

show the carrier injection direction at each electrode. LUMO,D and HOMO,D indicate LUMO and

HOMO level of electron donor (P3HT) while LUMO,A and HOMO,D corresponds to electron acceptor
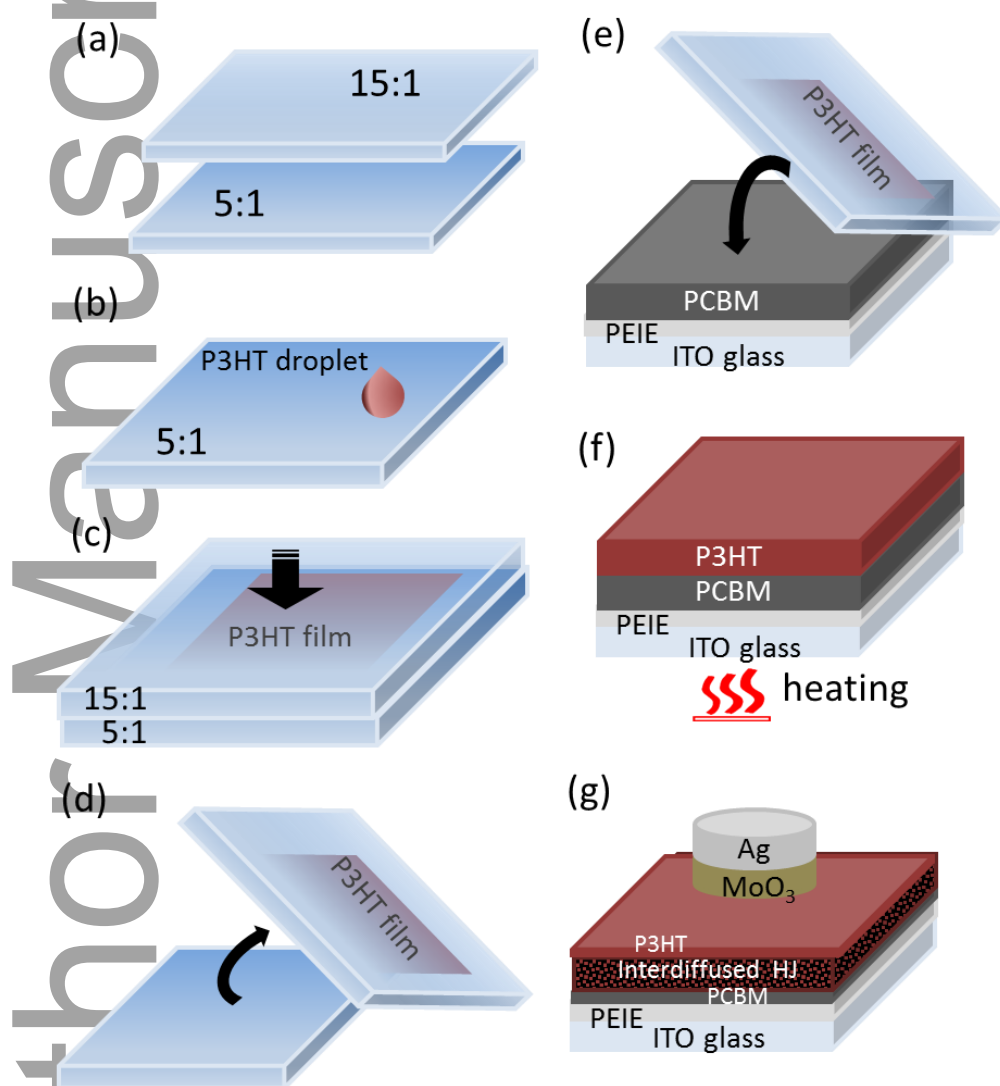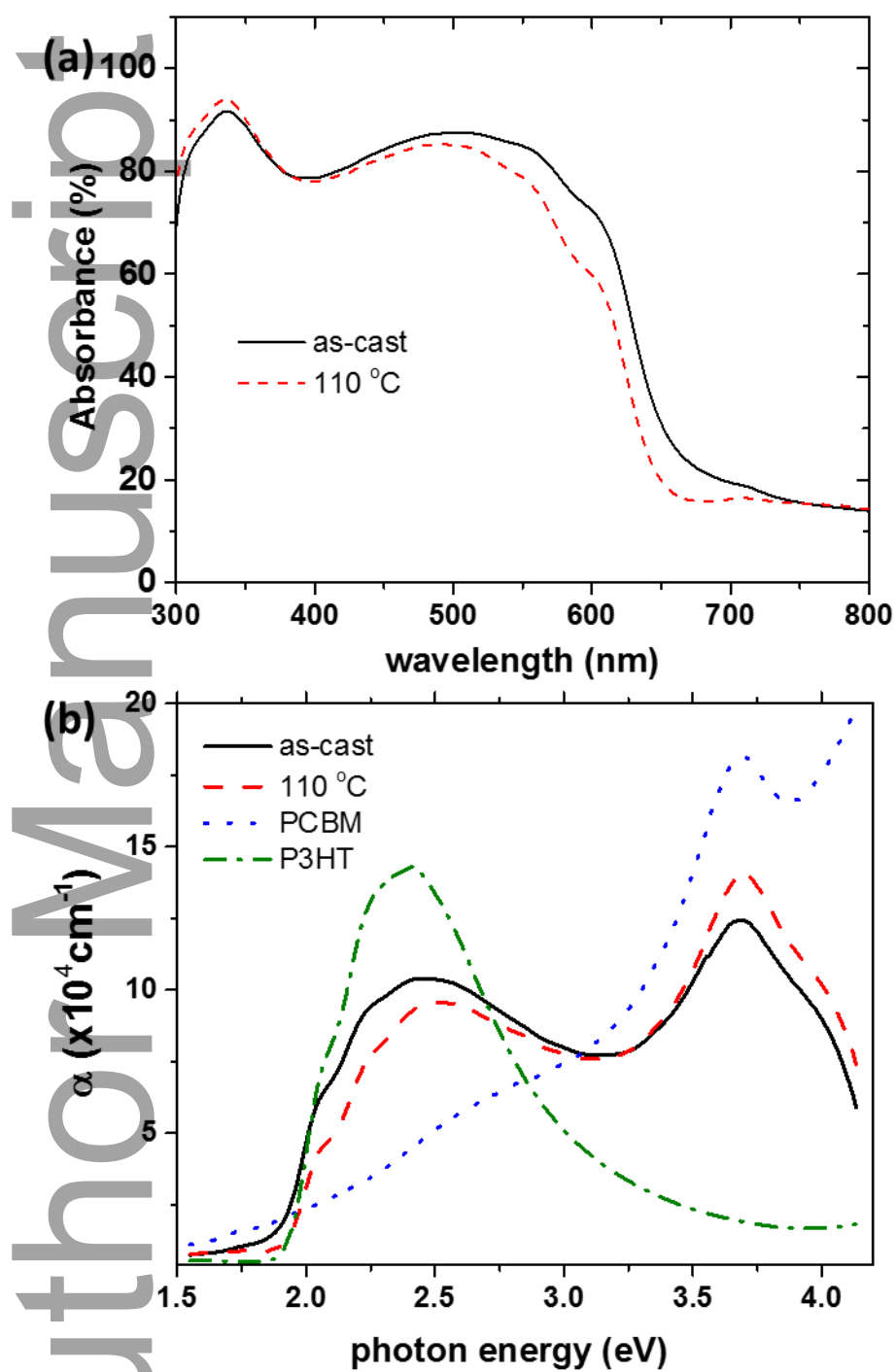
(PCBM)

Figure 2. Schematic illustration of proposed double transfer stamping (DTS) process for fabricating

bilayer heterojunction organic photodiodes: (a) Prepare PDMS stamps with different surface

energies. (b) Drop-cast P3HT droplet on the PDMS stamp (5:1) with the lowest surface energy. (c) Squeeze the drop-casted solution with the high surface energy PDMS stamp (15:1) to form a uniform film. (d) Detach PDMS stamp, transferring the film to the 15:1 stamp. (e) Transfer the P3HT film from the stamp onto a PCBM/PEIE/ITO substrate. (f) Heat substrate to allow interdiffusion of PCBM into P3HT (g) Complete the device fabrication by depositing MoO_3/Ag anode. All the processes are done inside a N_2-filled glove box to prevent degradation.

Figure 3. (a) Absorbance spectra of as-cast and 110 ^{o}C BiHJ active layer. The thicknesses of the films are 200 nm. (b) Absorption coefficient plot versus photon energy for as-cast, 110 ^{o}C, PCBM and P3HT films deposited on glass substrates.
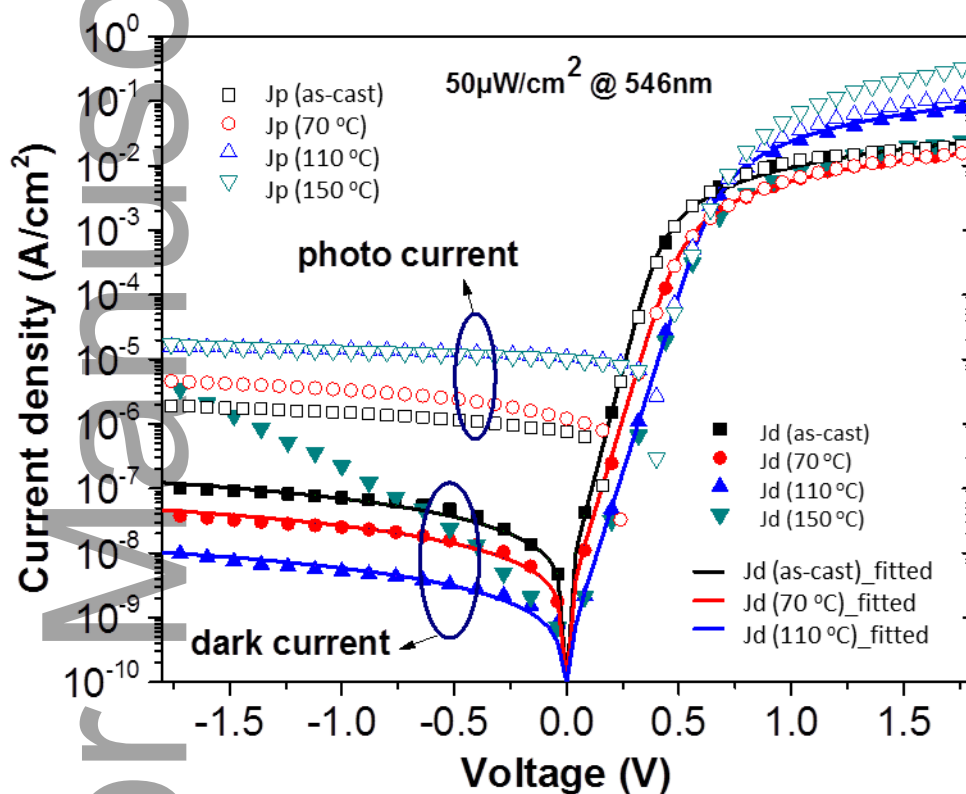

Figure 4. Dark (filled symbols) and illuminated (open symbols) current density (*J*) versus voltage (*V*) characteristics for OPDs with different annealing conditions. Light illumination at 50µW/cm^{2} and 546nm was used. The solid lines indicate fits to the data (see text).
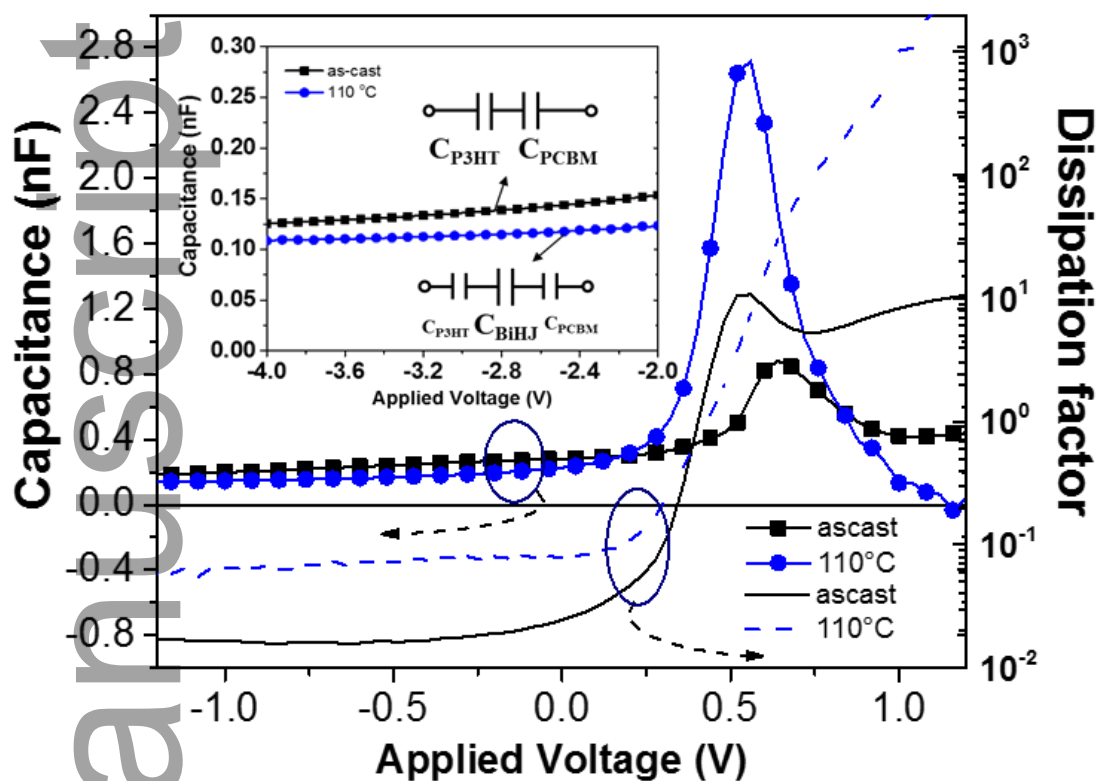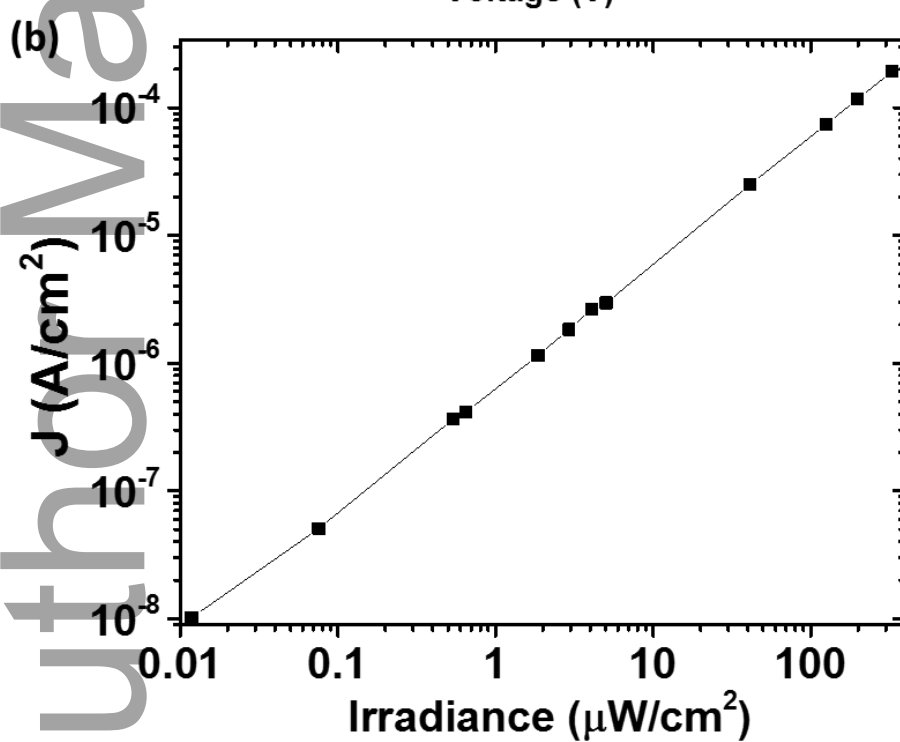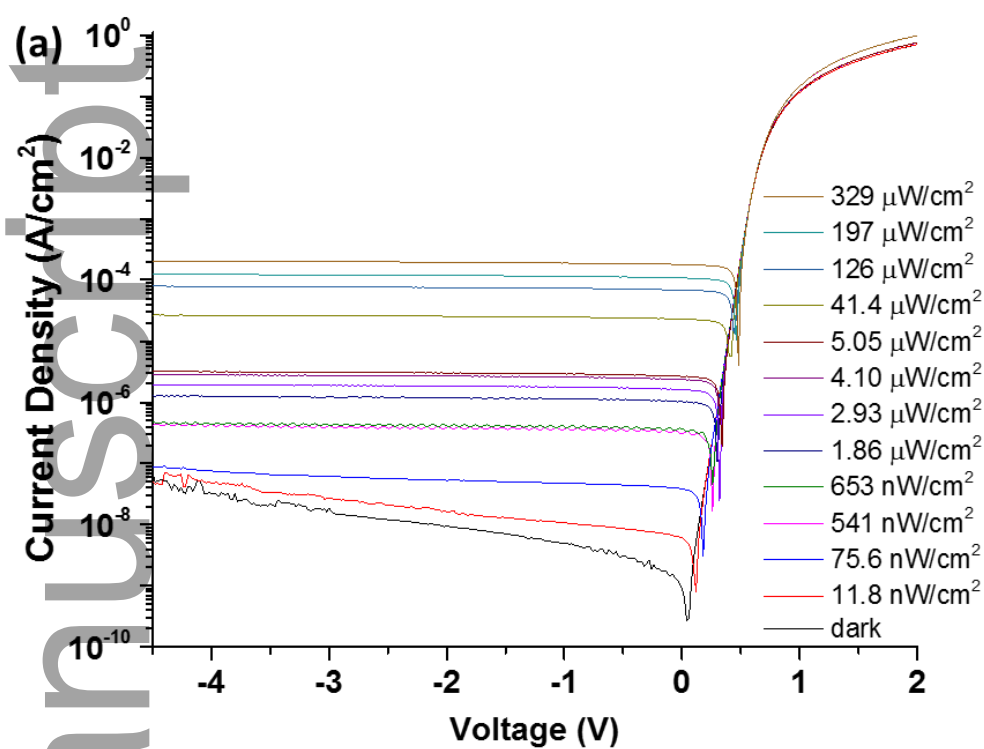
Figure 5. Capacitance-voltage (*C–V*) characteristics of the BiHJ OPDs with as-cast and 110 ^{o}C annealing conditions along with dissipation factor (*D* = 1/ωRC, R is device resistance). Inset: *C–V* characteristics from -2 V to -4 V. Also shown are equivalent capacitance circuits for each device. Negative bias was applied to anode electrode.

(a)

Legend (top to bottom):
- 329 $\mu W/cm^2$
- 197 $\mu W/cm^2$
- 126 $\mu W/cm^2$
- 41.4 $\mu W/cm^2$
- 5.05 $\mu W/cm^2$
- 4.10 $\mu W/cm^2$
- 2.93 $\mu W/cm^2$
- 1.86 $\mu W/cm^2$
- 653 nW/cm^2
- 541 nW/cm^2
- 75.6 nW/cm^2
- 11.8 nW/cm^2
- dark

(b)

Figure 6. (a) *J-V* curve of the BiHJ OPD with 110 ^{o}C annealing condition under various light intensities at 546 nm wavelength. (b) Variation of the photocurrent with irradiance of the BiHJ OPD annealed at 110 ^{o}C under monochromatic light of 546 nm and reverse bias of 1.5 V. Negative bias was applied to anode electrode.
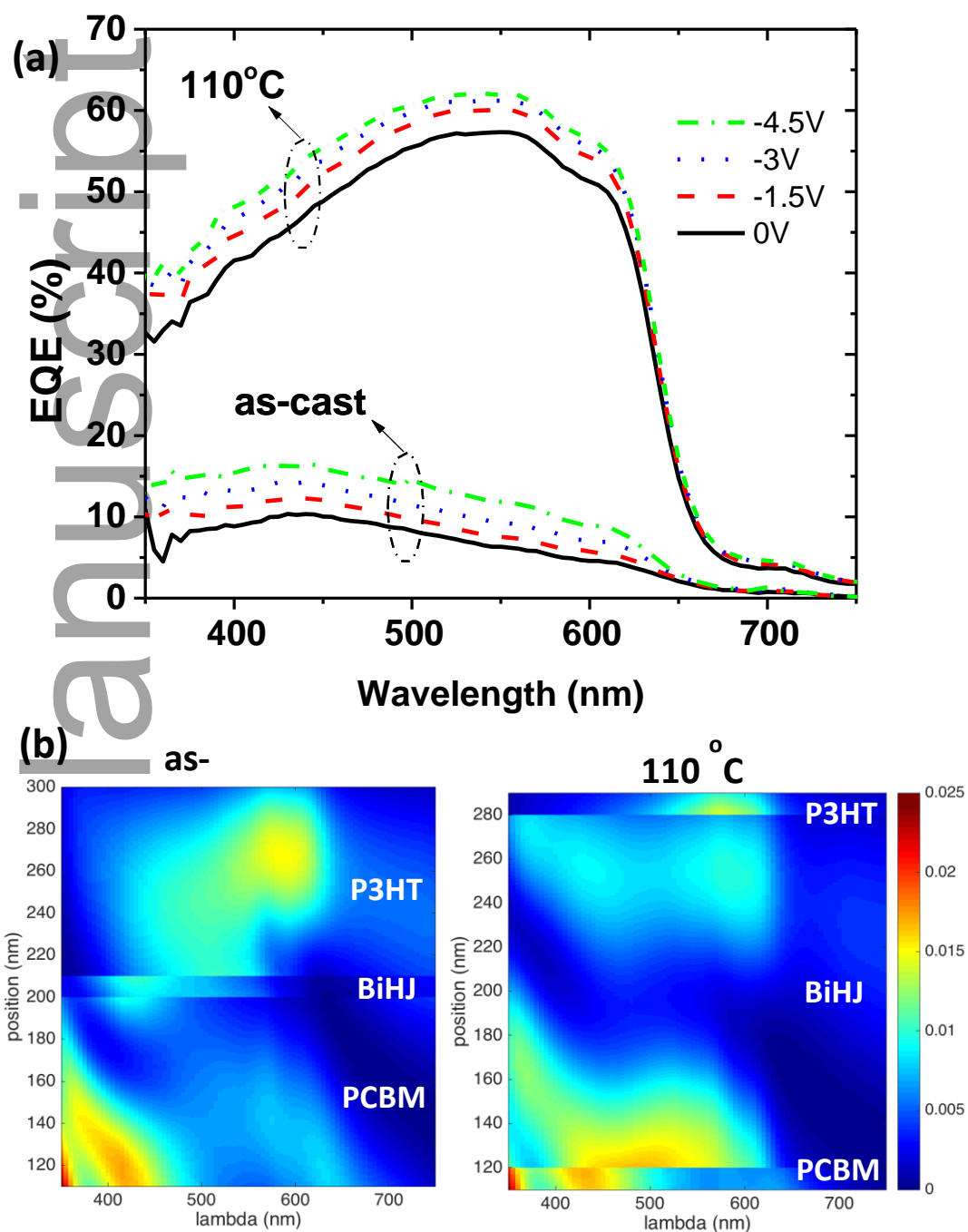
Figure 7. (a) External quantum efficiency (*EQE*) spectrum of the BiHJ OPDs under various reverse

biases with as-cast and 110 °C annealing conditions. (b) Absorbed optical power distribution of the

BiHJ OPD active layers with as-cast (left) and 110 $^{\circ}$C (right) annealing conditions. The light is illuminated through the substrate.

A novel double transfer stamping method for the fabrication of a bilayer, interdiffused organic photodetector is demonstrated. The concept leads to a device having both a low dark current densities of 7.7 nA/cm^2 and high EQE of 60 % through optimized segregation of electron donor and acceptor materials within the active layer.